

# Rotational Diffusion Anisotropy and Local Backbone Dynamics of Carbon Monoxide-Bound *Rhodobacter capsulatus* Cytochrome *c'*

Pascale Tsan,<sup>†</sup> Jean-Christophe Hus, Michael Caffrey,<sup>‡</sup> Dominique Marion, and Martin Blackledge\*

Contribution from the Institut de Biologie Structurale, Jean-Pierre Ebel C.N.R.S.–C.E.A., 41, Rue Jules Horowitz, 38027 Grenoble Cedex, France

Received October 12, 1999. Revised Manuscript Received March 15, 2000

**Abstract:** The rotational diffusion and backbone dynamics of the carbon monoxide-bound *Rhodobacter capsulatus* cytochrome *c'* have been investigated using heteronuclear NMR spectroscopy. This protein consists of a four-helix bundle motif and a histidine-heme binding domain and has been shown to form a symmetric dimer in the crystal state. <sup>15</sup>N relaxation measurements reveal that an asymmetric tensor is necessary to describe overall rotational diffusion of the protein, showing a significant improvement compared to analysis using either isotropic and axially symmetric tensors. This analysis indicates that the molecule undergoes significant anisotropic reorientation with a diffusion tensor having principal components  $\{1.37 \pm 0.05, 1.68 \pm 0.06, 2.13 \pm 0.07\} \times 10^7 \text{ s}^{-1}$ . Hydrodynamic calculations performed on the crystal structure predict values of  $\{1.400, 1.45, 2.12\} \times 10^7 \text{ s}^{-1}$  when a solvent shell of 3.0 Å is included in the calculation. Comparison of the principal axes with the symmetry axes of the dimeric structure derived from X-ray crystallography provides unambiguous evidence that the molecule is monomeric in the solution state. Lipari–Szabo-type mobility parameters extracted when using the anisotropic description of overall tumbling are found to differ considerably from those found assuming isotropic global reorientation, where the internal dynamics of NH vectors present in helical regions of the molecule exhibit clear periodicity due to their orientation relative to the diffusion tensor. In addition, the relaxation properties of helix I are less well reproduced than those of the other three helices, implying a different orientation of this helix compared to that found in the crystal state, possibly due to the volume of the different ligands present in the two forms of the protein. Using restrained molecular dynamics and energy minimization with respect to the relaxation rate ratios, we have quantified the difference in the orientation of this helix and find that a significant reorientation is necessary to fulfill the measured relaxation rates.

## Introduction

Heteronuclear NMR spin relaxation is a proven tool for the characterization of molecular dynamics.<sup>1,2</sup> Data are normally interpreted using an abstract model-free dynamics formalism<sup>3</sup> or by simple matrix inversion, to provide direct samples of the spectral density function<sup>4</sup> of NH vectors along the peptide chain. In the model-free approach, mobility is characterized using an order parameter  $S^2$ , which may be interpreted as the amplitude of the motion and a correlation time  $\tau_1$ —the characteristic time constant of this motion. The physical nature of the mobility is not constrained, but the internal and global motions are assumed to be independent, and the overall and internal autocorrelation functions are assumed to have an exponential nature. The interpretation has been further extended to take account of two uncoupled internal motions and hence three independent terms in the time correlation function.<sup>5</sup>

In order for this interpretation to be accurate, it is essential to correctly evaluate the contribution to relaxation due to overall rotational tumbling. This is particularly important in the presence of anisotropic rotational diffusion, as relaxation rates then depend strongly on the direction of the individual relaxation interactions.<sup>6</sup> This dependence has, indeed, been successfully exploited in recent years to accurately determine the hydrodynamic properties of proteins in solution.<sup>7–12</sup> Clearly, this double dependence of spin relaxation on internal motion and NH vector orientation can lead to potential problems if one of the two contributions is not correctly taken into account. It has, indeed, been shown that fictive slow motions can be evoked if isotropic motion is assumed in the presence of anisotropic overall motion.<sup>13</sup>

\* To whom correspondence should be addressed.

<sup>†</sup> Current address: Biological NMR Centre, Department of Biochemistry, Leicester University, University Road, Leicester LE1 7RH, U.K.

<sup>‡</sup> Current address: Department of Biochemistry and Molecular Biology, University of Illinois at Chicago, Chicago, IL 60612.

(1) Abragam, A. *The Principles of Nuclear Magnetism*; Oxford University Press: Oxford, 1961.

(2) Kay, L. E.; Torchia, D. A.; Bax, A. *Biochemistry* **1989**, *28*, 8972.

(3) (a) Lipari, G.; Szabo, A. *J. Am. Chem. Soc.* **1982**, *104*, 4546. (b) Lipari, G.; Szabo, A. *J. Am. Chem. Soc.* **1982**, *104*, 4559.

(4) (a) Peng, J.; Wagner, G. *Biochemistry* **1992**, *31*, 8571. (b) Peng, J.; Wagner, G. *Biochemistry* **1995**, *34*, 16733.

(5) Clore, G. M.; Szabo, A.; Bax, A.; Kay, L. E.; Driscoll, P. C.; Gronenborn, A. M. *J. Am. Chem. Soc.* **1990**, *112*, 4989.

(6) Woessner, D. E. *J. Chem. Phys.* **1962**, *37*, 647.

(7) Barbato, G.; Ikura, M.; Kay, L. E.; Pastor, R. W.; Bax, A. *Biochemistry* **1992**, *31*, 5269.

(8) Brüschweiler, R.; Liao, X.; Wright, P. E. *Science* **1995**, *268*, 886.

(9) Tjandra, N.; Feller, S. E.; Pastor, R. W.; Bax, A. *J. Am. Chem. Soc.* **1995**, *117*, 12562.

(10) Zheng, Z.; Czaplicki, J.; Jardetzky, O. *Biochemistry* **1995**, *34*, 5212.

(11) Lee, L. K.; Rance, M.; Chazin, W. J.; Palmer, A. G. *J. Biomol. NMR* **1997**, *9*, 287.

(12) Cordier, F.; Caffrey, M.; Brutscher, B.; Cusanovich, M.; Marion, D.; Blackledge, M. *J. Mol. Biol.* **1998**, *281*, 341.

(13) Schurr, J. M.; Babcock, H. P.; Fujimoto, B. S. *J. Magn. Reson. Ser. B* **1994**, *105*, 211.

In this paper we present a detailed analysis of the local and global dynamic properties of the highly anisotropic protein, the cytochrome *c'* from *Rhodobacter capsulatus*. Cytochromes *c'* form a subclass (IIa) of cytochromes found in a wide range of photosynthetic and denitrifying bacteria.<sup>14–16</sup> Although their precise biological function is not known, they function as electron transporters with oxidation–reduction potentials in the range from 0 to +150 mV. The primary sequence homology among class IIa cytochromes is relatively low (around 20%),<sup>17</sup> although all are characterized by a pentacoordinated heme, binding close to the C-terminus and a left-handed-twisted four- $\alpha$ -helix bundle fold. The three-dimensional structure of several cytochromes *c'* has been solved in recent years: cyt *c'* from *Rhodospirillum molischianum* (RMCP),<sup>18,19</sup> *Rhodospirillum rubrum* (RRCP),<sup>20</sup> *Chromatium vinosum* (CVCP),<sup>21</sup> two polymorphs of *Rhodobacter capsulatus* (RCCP),<sup>22</sup> *Alcaligenes denitrificans* (ADCP),<sup>23</sup> *Rhodocyclus gelatinosus* (RGCP),<sup>24</sup> and *Rhodopseudomonas palustris*.<sup>25</sup> All cytochromes *c'* have been found to be dimers comprising two identical subunits of approximately 14 kD, except for the protein isolated from *Rhodopseudomonas palustris*, which is monomeric. The cytochrome *c'* from *Rhodobacter capsulatus* has also been shown to exist in a monomer/dimer equilibrium in solution<sup>26</sup> but nevertheless crystallizes as a dimer with a unique relative subunit orientation compared to other members of the cytochrome *c'* family. The resultant reduced surface area of the dimer interface has been correlated with this lower propensity to dimerize.<sup>22</sup> Due to the absence of a sixth ligand from the peptide chain of the molecule, the cytochrome *c'* can bind small molecules at the heme iron. The dimerization state of the protein is of particular interest in this respect, as dimer dissociation has been shown to be related to the differential ligand-binding properties of the various forms of the molecule.<sup>27–31</sup> In addition to the investigation of the local flexibility of the cytochrome *c'*, we use <sup>15</sup>N relaxation data to investigate the oligomerization state of the CO bound form of the protein in solution.

(14) Bartsch, R. G. *Cytochromes*. In *The Photosynthetic Bacteria*; Clayton R. K., Sistrom, W. R., Eds; Plenum: New York, 1978; pp 249–280.

(15) Meyer, T. E.; Kamen, M. D. *Adv. Protein Chem.* **1982**, *35*, 105.

(16) Cusanovich, M. A.; Meyer, T. E.; Tollin, G. *Adv. Bioinorg. Chem.* **1987**, *7*, 37.

(17) Moore, G. R.; Pettigrew, G. W. *Cytochromes c—evolutionary, structural and physicochemical aspects*; Springer-Verlag: Berlin–Heidelberg, 1990.

(18) Weber, P. C.; Howard, A.; Xuong, N. H.; Salemme, F. R. *J. Mol. Biol.* **1981**, *153*, 399.

(19) Finzel, B. C.; Weber, P. C.; Hardman, K. D.; Salemme, F. R. *J. Mol. Biol.* **1985**, *186*, 627.

(20) Yazui, M.; Harada, S.; Kai, N.; Kusunaki, M.; Matsuura, Y. *J. Biochem.* **1992**, *111*, 317.

(21) Ren, Z.; Meyer, T. E.; McRee, D. E. *J. Mol. Biol.* **1993**, *234*, 433.

(22) Tahirov, T. H.; Shintaro, M.; Meyer, T. E.; Cusanovich, M.; Higuchi, Y.; Yasuoka, N. *J. Mol. Biol.* **1996**, *259*, 467.

(23) Dobbs, A. J.; Anderson, B. F.; Faber, H. R.; Baker, E. *Acta Crystallogr. Sect. D* **1996**, *52*, 356.

(24) Archer, M.; Banci, L.; Dikaya, E.; Romao, M. *J. Biol. Inorg. Chem.* **1997**, *2*, 611.

(25) Shibata, N.; Iba, S.; Misaki, S.; Meyer, T. E.; Bartsch, R. G.; Cusanovich, M. A.; Morimoto, Y.; Higuchi, Y.; Yasuoka, N. *J. Mol. Biol.* **1998**, *284*, 751.

(26) Cusanovich, M. A. *Biochim. Biophys. Acta* **1971**, *236*, 238.

(27) Taniguchi, S.; Kamen, M. D. *Biochim. Biophys. Acta* **1963**, *74*, 438.

(28) Kassner, R. J.; Kykta, M. G.; Cusanovich, M. A. *Biochim. Biophys. Acta* **1985**, *831*, 155.

(29) Patel, M. J.; Kassner, R. J.; Meyer, T. E.; Cusanovich, M. *Biochemistry* **1989**, *28*, 2140.

(30) Tahirov, T. H.; Shintaro, M.; Meyer, T. E.; Cusanovich, M.; Higuchi, Y.; Yasuoka, N. *Nat. Struct. Biol.* **1996**, *3*, 459.

(31) Doyle, M. L.; Gill, S. J.; Cusanovich, M. A. *Biochemistry* **1986**, *25*, 2509.

## Materials and Methods

**Sample Preparation.** All NMR experiments were performed using <sup>15</sup>N-labeled sample prepared as described recently.<sup>32</sup> To prepare the CO-bound version, the sample was concentrated at 277 K to 7 mM in 100 mM PO<sub>4</sub> at pH 6.0, and then oxygen was removed by passing argon gas over the surface of the solution for 15 min followed by saturation with CO and reduction using 10 mg of sodium dithionite (Janssen Chimica).

**NMR Spectroscopy.** We have recently assigned the <sup>1</sup>H and <sup>15</sup>N NMR resonances of the diamagnetic CO-bound form of RCCP strain M1131,<sup>33</sup> which is the form studied here.

**Relaxation Experiments.** Relaxation measurements were performed on the <sup>15</sup>N-labeled sample at 300 K, using a Bruker AMX 600-MHz (<sup>1</sup>H) spectrometer equipped with a triple-resonance gradient probe. The <sup>15</sup>N *R*<sub>1</sub> and *R*<sub>1ρ</sub> relaxation rates and <sup>1</sup>H–<sup>15</sup>N NOE measurements were carried out using the classical <sup>1</sup>H-detected pulse sequence based on established methods<sup>34</sup> and described in detail elsewhere.<sup>12</sup>

The relaxation rates *R*<sub>1</sub> and *R*<sub>1ρ</sub> were sampled at the following time points: for *R*<sub>1</sub>, 20, 40, 80, 160, 380, 620, 780, 960, and 1190 ms; for *R*<sub>1ρ</sub>, 20, 40, 60, 80, 100, 120, 160, and 200 ms. A recycle delay 2.5 s was used. For *R*<sub>1ρ</sub>, a <sup>15</sup>N spin-lock field was used during the relaxation decay time, with a strength of about 2.0 kHz for both fields. *R*<sub>1ρ</sub> values were corrected to compensate for resonance offset effects using

$$1/T_{1\rho} = \cos^2(\theta)/T_2 + \sin^2(\theta)/T_1 \quad (1)$$

with  $\theta = \tan^{-1}(\Omega_N/\gamma_N B_1)$ , where  $\Omega_N$  is the resonance offset and  $\gamma_N B_1$  is the strength of the spin-lock field. The *R*<sub>2</sub> values are then directly extracted for each residue from *R*<sub>1ρ</sub> and *R*<sub>1</sub> data, and  $\theta$ . A field strength of about 2.0 kHz was used to compromise offset and probe heating. Temperature control devices were calibrated using a glycerol sample.

Resonance intensities were treated using the Levenberg–Marquardt minimization algorithm as previously described to derive <sup>15</sup>N *R*<sub>1</sub> and *R*<sub>1ρ</sub> relaxation rates. The NOE values were derived from the ratio between the intensities in the “saturation spectrum” and in the “reference spectrum”.

**Relaxation Data Analysis.** The <sup>15</sup>N heteronuclear relaxation parameters *R*<sub>1</sub>, *R*<sub>2</sub>, and NOE depend on the spectral density function *J*( $\omega$ ) in the following manner:

$$R_1 = d^2[J(\omega_H - \omega_N) + 3J(\omega_N) + 6J(\omega_H + \omega_N)] + c^2J(\omega_N) \quad (2a)$$

$$R_2 = (d^2/2)[4J(0) + J(\omega_H - \omega_N) + 3J(\omega_N) + 6J(\omega_H + \omega_N) + 6J(\omega_H)] + (c^2/6)[4J(0) + J(\omega_N)] \quad (2b)$$

$$\text{NOE} = 1 + d^2\gamma_H/\gamma_N[6J(\omega_H + \omega_N) - J(\omega_H - \omega_N)]/R_1 \quad (2c)$$

where

$$d^2 = \langle^1/_{10}\rangle\gamma_H^2/\gamma_N^2(h/2\pi)^2\langle r_{\text{NH}}^{-3}\rangle^2$$

and

$$c^2 = \langle^2/_{15}\rangle\omega_N^2(\sigma_{\parallel} - \sigma_{\perp})^2$$

where *h* is Planck's constant,  $\gamma_H$  and  $\gamma_N$  are the gyromagnetic ratios of <sup>1</sup>H and <sup>15</sup>N, respectively,  $\omega_H$  and  $\omega_N$  are their Larmor frequencies, and *r*<sub>NH</sub> is the internuclear distance (assumed to average to 1.01 Å).  $\sigma_{\parallel}$  and  $\sigma_{\perp}$  are the parallel and perpendicular components, respectively, of the axially symmetric <sup>15</sup>N chemical shift tensor (approximated to –170 ppm<sup>35</sup>), which is assumed to be coaxial with respect to the dipolar interaction.

(32) Caffrey, M.; Simorre, J.-P.; Brutscher, B.; Cusanovich, M. A.; Marion, D. *Biochemistry* **1995**, *34*, 5904.

(33) Tsan, P. Ph.D. Thesis, Université Joseph Fourier, Grenoble, France, 1998.

(34) Farrow, N. A.; Muhandiram, R.; Singer, A. U.; Pascal, S. M.; Kay, C. M.; Gish, G.; Shoelson, S. E.; Pawson, T.; Forman-Kay, J. D.; Kay, L. E. *Biochemistry* **1994**, *33*, 5984.

(35) Tjandra, N.; Wingfield, P.; Stahl, S.; Bax, A. *J. Biomol. NMR* **1996**, *8*, 273.

In the case of isotropic tumbling of the molecule, the model-free spectral density function is defined by

$$J(\omega) = S_2^2 \left\{ S_1^2 \frac{\tau_c}{1 + (\omega\tau_c)^2} + (1 - S_1^2) \frac{\tau'}{1 + (\omega\tau')^2} \right\} \quad \text{with} \\ \tau' = \frac{\tau_c \tau_i}{\tau_c + \tau_i} \quad (3)$$

where  $\tau_c$  is the overall correlation time of the molecule.

Using the Lipari–Szabo model-free approach,<sup>3</sup>  $J(\omega)$  is derived assuming  $S_2^2 = 1$ . The generalized order parameter  $S_1^2 = S^2$  describes the amplitude of the fast internal motion and  $\tau'$  the effective correlation time for fast internal motions. A second slower internal motion may be necessary<sup>5</sup>—this movement is characterized by  $S_1^2 = S_s^2$  and  $\tau_i$ , the order parameter and internal correlation time, respectively, for the slow internal motion. The correlation time of the fast motion is assumed to be negligible with regard to the measured relaxation parameters which are affected only by the order parameter  $S_2^2 = S^2$  ( $S^2 = S_s^2 S_f^2$ ) describing the rapid librational motion.

**Determination of Motional Parameters.** All data analysis was performed using programs written in the laboratory and described in greater detail elsewhere.<sup>12</sup> The following five models are iteratively tested, starting with the simplest model and invoking more complex models until the proposed model could give rise to the measured relaxation rates within 95% confidence limits: (1)  $S^2$ ; (2)  $S^2$ ,  $\tau_i$ ; (3)  $S^2$ ,  $R_{ex}$ ; (4)  $S^2$ ,  $\tau_i$ ,  $R_{ex}$ ; and (5)  $S_f^2$ ,  $S_s^2$ ,  $\tau_i$ . In model 1, motions on the fast time scale are too fast (<20 ps) to be characterized and affect  $R_1$  and  $R_2$  in a similar way. In model 2, internal motion is relaxation active. In models 3 and 4,  $R_{ex}$  contributes to  $R_2$ . Model 5 refers to the extended model described above.

Sets of relaxation data were fitted to dynamic models, using the optimized global correlation time (vide infra) by minimizing the function

$$\chi^2 = \sum_i \left\{ \frac{R_{i,n}^{\text{meas}} - R_{i,n}^{\text{calc}}}{\sigma_{i,n}^{\text{meas}}} \right\}^2 \quad (4)$$

where  $i$  represents the relaxation parameters used in the calculation.  $R_{i,n}^{\text{meas}}$ ,  $R_{i,n}^{\text{calc}}$ , and  $\sigma_{i,n}^{\text{meas}}$  are the experimental and calculated relaxation rates/NOE and the estimated experimental uncertainty of  $R_{i,n}^{\text{meas}}$ , respectively. Model selection is based on 500 Monte Carlo simulations to characterize the random variation in the fit, to provide probability statistics and estimate uncertainty. An  $F$  characteristic is used to judge the statistical significance of introducing an additional parameter to model 1.  $F$  is defined as<sup>36</sup>

$$F = \frac{(N - n)\{\chi_m^2 - \chi_n^2\}}{(n - m)\chi_n^2} \quad (5)$$

for the comparison of models fitting  $N$  variables with  $m$  and  $n$  parameters. In the case where the reduction of  $\chi^2$  was less than the  $\alpha = 0.20$  critical value for random statistical improvement, we have rejected the more complex model and proposed the model 1 parameterization.

**Anisotropic Tumbling: Fitting of the Anisotropic Rotational Diffusion Tensor.** The spectral density function describing anisotropic rotational diffusion<sup>6</sup> is given by

$$J(\omega) = \sum_j \left\{ \frac{A_j \tau_j}{1 + (\omega\tau_j)^2} \right\} \quad (6)$$

where

(36) Devore, J. *Probability and Statistics for Engineering and the Sciences*; Brooks/Cole Publishing Co.: Monterey, CA, 1982.

$$A_1 = 3\mathbf{y}^2\mathbf{z}^2, \quad A_2 = 3\mathbf{x}^2\mathbf{z}^2, \quad A_3 = 3\mathbf{x}^2\mathbf{y}^2$$

$$A_{4,5} = 0.25\{3(\mathbf{x}^4 + \mathbf{y}^4 + \mathbf{z}^4) - 1\} \pm (1/12)\{\delta_x(3\mathbf{x}^4 + 6\mathbf{y}^2\mathbf{z}^2 - 1) + \delta_y(3\mathbf{y}^4 + 6\mathbf{x}^2\mathbf{z}^2 - 1) + \delta_z(3\mathbf{z}^4 + 6\mathbf{y}^2\mathbf{x}^2 - 1)\}$$

and

$$\tau_{1,2,3} = (4D_{xx} + D_{yy} + D_{zz})^{-1}, \quad (D_{xx} + 4D_{yy} + D_{zz})^{-1}, \\ (D_{xx} + D_{yy} + 4D_{zz})^{-1}$$

$$\tau_{4,5} = (6D_{\text{iso}}^2 \pm 6(D_{\text{iso}}^2 - L^2)^{1/2})$$

$$D_{\text{iso}} = (D_{xx} + D_{yy} + D_{zz})/3$$

$$L^2 = (D_{xx}D_{yy} + D_{xx}D_{zz} + D_{yy}D_{zz})/3$$

and

$$\delta_m = (D_{mm} - D_{\text{iso}})/(D_{\text{iso}}^2 - L^2)^{1/2}$$

$m = (x,y,z)$  and  $(\mathbf{x},\mathbf{y},\mathbf{z})$  are the direction cosines of the N–H vector in the principal axis frame of the diffusion tensor. Six parameters ( $D_{xx}$ ,  $D_{yy}$ ,  $D_{zz}$ ,  $\theta$ ,  $\phi$ , and  $\psi$ ) are optimized, describing the orientation and amplitude of the principal components of the diffusion tensor in the chosen molecular frame. For axially symmetric diffusion,  $D_{\perp} = D_{xx} = D_{yy}$ ,  $D_{\parallel} = D_{zz}$ ,  $\tau_{1,2,3} = (6D_{\perp})^{-1}$ ,  $(5D_{\perp} + D_{\parallel})^{-1}$ ,  $(2D_{\perp} + 4D_{\parallel})^{-1}$ , and  $A_{1,2,3} = (3 \cos^2 \alpha - 1)^2/4$ ,  $3 \sin^2 \alpha \cos^2 \alpha$ ,  $(3/4)\sin^4 \alpha$ , where  $\alpha$  is the angle between the N–H bond and the unique axis of the diffusion tensor. Four parameters are optimized ( $D_{\perp}$ ,  $D_{\parallel}$ ,  $\theta$ , and  $\phi$ ) in this case. The diffusion parameters are extracted by minimizing

$$\chi^2 = \sum_n \{ [(R_2^{\text{meas}}/R_1^{\text{meas}}) - (R_2^{\text{calc}}/R_1^{\text{calc}})]_n / \sigma_n \}^2 \quad (7)$$

where  $\sigma$  is the uncertainty in the experimental  $R_2/R_1$  ratio.

The summation is performed over the residues in the helices. Cartesian coordinates of the appropriate vectors were taken from either the *n*-butyl isocyanide-bound<sup>30</sup> (PDB code 1nbb) or the free<sup>22</sup> (PDB code 1rcp) form of cytochrome *c'* from *Rhodobacter capsulatus*. The fit of the diffusion tensor components and orientation is performed using a simulated annealing algorithm developed in our laboratory; this program (TENSOR) allows the complete exploration of the available parametric space.<sup>37</sup>

The program also performs Monte Carlo simulations to evaluate the uncertainty of the fitted diffusion parameters and to test the significance of the fit against estimated experimental error. Here, 1000 simulated sets of  $R_1$  and  $R_2$  values for each residue were selected from Gaussian noise distributions of width  $\sigma_R$  and centered on the optimal rates back-calculated from the best-fit anisotropic diffusion parameters.

The axially symmetric and asymmetric fits require four- and six-parameter fits, respectively, to model the rotational diffusion. It is therefore important to test the significance of the improved fit to ensure that reduced  $\chi^2$  is not simply due to the introduction of supplementary parameters into the model. This is tested by calculating the random statistical improvement achieved when noise simulations assuming axial symmetry are fitted using an asymmetric model. Distinction between the different diffusion models is achieved by calculating the function  $F$  (vide supra) to test the justification of including more parameters into the fit. If the  $F$  statistic is greater than a given threshold, then the improved model is statistically relevant. This can also be expressed as a probability  $p$  that the improvement is due to random fluctuation.

**Extraction of Global Correlation Time.** The global isotropic correlation time has been optimized by treating the residues exhibiting no obvious signs of relaxation active mobility (in this case, spins present

(37) Dosset, P.; Hus, J.-C.; Blackledge, M. J.; Marion, D. *J. Biomol. NMR* 2000, 16, 23.

in  $\alpha$ -helical secondary structural motifs). The diffusion tensor was optimized using the algorithm presented above, assuming isotropic motion.

**Anisotropy and Internal Mobility.** The orientation and the components of the diffusion tensor were introduced into the first term of the general spectral density function:

$$J(\omega) \approx S^2 \sum_j \frac{A_j \tau_j}{1 + (\omega\tau_j)^2} + (1 - S^2) \frac{\tau'}{1 + (\omega\tau')^2} \quad \text{with} \quad \tau'^{-1} = 6D + \tau_i^{-1} \quad (8)$$

This definition was used to characterize the local mobility in terms of the Lipari–Szabo formalism. Fast internal motion ( $\tau_i \ll (6D)^{-1}$ ) is assumed to be independent of overall rotational tumbling and is thus analogous to the isotropic Lipari–Szabo model-free approach. Statistical testing of the significance of the derived models was determined using the same criteria for model selection as in the isotropic case.

**Hydrodynamic Calculations.** Hydrodynamic calculations were performed using the program DIFFC in the package DASHA.<sup>38</sup> The program uses the bead model:<sup>39</sup> a description of the protein as a matrix of points with defined friction coefficients, whose hydrodynamic behavior is described by the modified Oseen tensor for overlapping or nonoverlapping beads of different radii. The components of the global rotational diffusion tensor have been calculated for a series of hydration shells added to the structure, using the InsightII program. The hydration shell was optimized by matching the calculated effective correlation time ( $1/6D$ ) to the experimentally determined effective isotropic correlation time ( $\tau_c$ ) of the molecule. The temperature was set to 300 K for all calculations. Radii of friction points are scaled according to the accessible surface areas,<sup>40</sup> and beads representing all heavy atomic positions with van der Waals radii were used.

**Structural Modeling Using Relaxation as Constraints.** To model the structure of the CO-ligated cytochrome *c'*, we have performed the following simple calculations. All simulations were performed using Discover with the AMBER4 force field,<sup>41</sup> modified to incorporate parameters characterizing the CO and heme groups. Protons were added to the coordinates of the crystal structure of the ligand-free cytochrome *c'*, and the ligand CO was positioned appropriately as the sixth ligand. The structures were then energy-minimized with the heavy atoms fixed.

The relaxation rates were introduced into the structure calculation using the following energy term, which we have incorporated into the Discover code:<sup>42</sup>

$$E_{R_2R_1} = k_{R_2R_1} [(R_2^{\text{meas}}/R_1^{\text{meas}}) - (R_2^{\text{calc}}/R_1^{\text{calc}})]^2 / \sigma^2 \quad (9)$$

$\sigma$  is the experimental uncertainty in the relaxation rates.

The backbone atoms of the molecule were tethered to their initial positions by incorporating the additional energy term,

$$E_{\text{teth}} = k_{\text{teth}} \sum_i \sqrt{(x_i - x_i^0)^2} / N \quad (10)$$

into the potential energy function.  $x_i$  are the Cartesian coordinates of the atoms to be tethered and  $x_i^0$  the target coordinates. The force constant  $k_{\text{teth}}$  is used to restrain the  $N = 542$  atoms to the coordinates of the crystal structure. As this energy term is applied as a sum over all backbone atoms, global unfolding is avoided while local reorientation is allowed. Solvent effects were implicitly included using a distance-

(38) Orekhov, V. Y.; Nolde, D. E.; Golovanov, A. P.; Korzhnev, D. M.; Arseniev, A. S. *Appl. Magn. Reson.* **1995**, *9*, 581.

(39) Garcia de la Torre, P.; Bloomfield, V. A. *Q. Rev. Biophys.* **1981**, *14*, 81.

(40) Lee, B.; Richards, F. M. *J. Mol. Biol.* **1971**, *55*, 379.

(41) Pearlman, D. A.; Case, D. A.; Caldwell, J.C.; Seibel, G.L.; Singh, U. C.; Weiner, P.; Kollman, P. A. *AMBER 4.0*; University of California, San Francisco, 1991.

(42) Hus, J.-C.; Marion, D.; Blackledge, M. *J. Am. Chem. Soc.* **1999**, *121*, 2311.

dependent dielectric constant and reduced charges on solvent-exposed polar side chains.<sup>43</sup>

The rotational diffusion tensor was assumed to be that determined using all four helices. In our version of Discover, the rotational diffusion tensor **D** is incorporated as a four-point system representing the three orthogonal axes of the tensor. The protein was therefore initially fixed, and the orientation and eigenvalues of the tensor were optimized by minimizing the energy function given by eq 9 with the system representing **D** completely free to evolve. The tensor was then fixed, and the molecular coordinates were optimized with respect to the tethering potential restraining the overall form of the molecule and the relaxation rate potential. The relative contributions of the functions in eqs 9 and 10 were set to  $k_{\text{teth}} = 10.0 \text{ kcal mol}^{-1} \text{ \AA}^{-2}$  and  $k_{R_2R_1} = 10.0 \text{ kcal mol}^{-1}$ . The former applies to the whole molecule, while the latter is applied to each relaxation rate ratio and is therefore the dominant contribution. The relative weighting of these terms was estimated empirically. The system was then equilibrated at 300 K for 5 ps using direct velocity scaling, followed by a 10-ps sampling period during which the temperature was controlled using weak coupling to a thermal bath using a time constant of 0.1 ps.<sup>44</sup> The system was slowly cooled to 100 K over a period of 10 ps and energy minimized in the same force field. Nonbonded interactions were ignored beyond 11 Å, and a switching function applied from 9.5 to 11 Å and a time step of 1 fs were used for all molecular dynamics simulations. The calculation was repeated using different initial velocity distributions.

## Results and Discussion

**<sup>15</sup>N NMR Data Analysis.** Of the 126 protonated backbone nitrogens, 106 were available for relaxation measurements using <sup>1</sup>H–<sup>15</sup>N HSQC-like spectra. The average values and errors calculated by Monte Carlo simulations were  $1.25 \pm 0.04 \text{ s}^{-1}$  for  $R_1$ ,  $13.5 \pm 0.8 \text{ s}^{-1}$  for  $R_2$ , and  $0.80 \pm 0.04$  for NOE. The results for the measurements of the <sup>15</sup>N  $R_1$ ,  $R_2$ , and <sup>1</sup>H–<sup>15</sup>N NOE are shown in Figure 1 and are given as Supporting Information.

**Isotropic Tumbling—Model-Free Approach.** The initial estimation of the overall correlation time, assuming isotropic global reorientation, was derived from the mean  $R_2/R_1$  ratio as previously described.<sup>12</sup> This gives a value of  $\tau_c = 9.75 \pm 0.03 \text{ ns}$ . It should be noted that if we include only the residues present in the four helices in this calculation, the value is significantly higher ( $\tau_c = 10.47 \pm 0.03 \text{ ns}$ ) as the helices sample a restricted region of angular space (vide infra).

Internal mobility parameters derived using the model-free approach assuming isotropic rotational diffusion are shown in Figure 2. Of the 106 residues considered, the dynamic behavior of all but three can be modeled using the formalism available from the Lipari–Szabo approach. All three (Gly58, Ala73, and Ala76) are in loop regions, and none has a  $\chi^2$  higher than 2.08. Monte Carlo analysis of the motional models show the  $\alpha = 0.05$  critical values to be close to the expectation values throughout the data sets, indicating well-behaved error functions.

While the average order parameter ( $S^2 = 0.86 \pm 0.12$ ) is comparable to the expected value for a relatively rigid molecule, there is a marked fluctuation of  $S^2$  in the  $\alpha$ -helical regions which appears to follow a 3–4-residue periodicity with respect to the primary sequence. In addition, 42 of the 47 residues requiring a significant conformational exchange contribution for the relaxation rates to be adequately reproduced within the limits of experimental uncertainty are present in the four helical regions and follow a similar cyclic pattern. By contrast, some residues in the interhelical loop regions tend to show significant slow motion when this simple model of overall rotational diffusion is used.

(43) Singh, U. C.; Kollman, P. A. *J. Comput. Chem.* **1983**, *5*, 129.

(44) Berendsen, H.; Postma, J.P.; van Gunsteren, W.; DiNola, A.; Haak, J. J. *Chem. Phys.* **1984**, *81*, 3684.

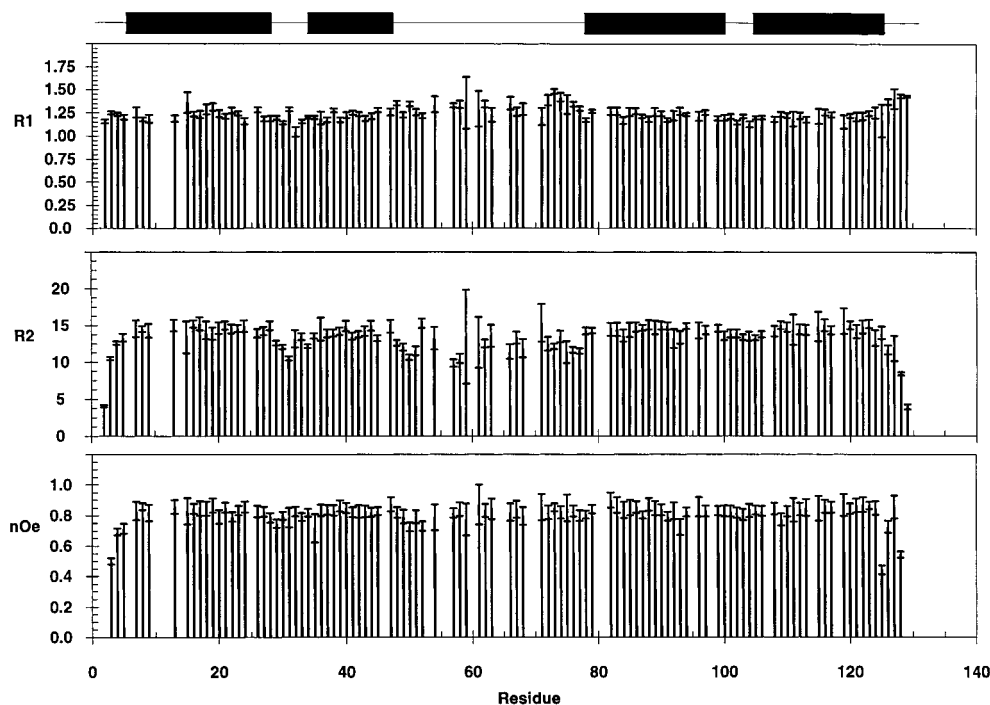


**Figure 1.** Experimental values of relaxation rates and associated uncertainties for cytochrome *c'* at 600 MHz with respect to protein sequence: (top)  $R_1$  ( $s^{-1}$ ), (middle)  $R_2$  ( $s^{-1}$ ), and (bottom) heteronuclear NOE. The position of the helices with respect to the primary sequence is shown above the figure.

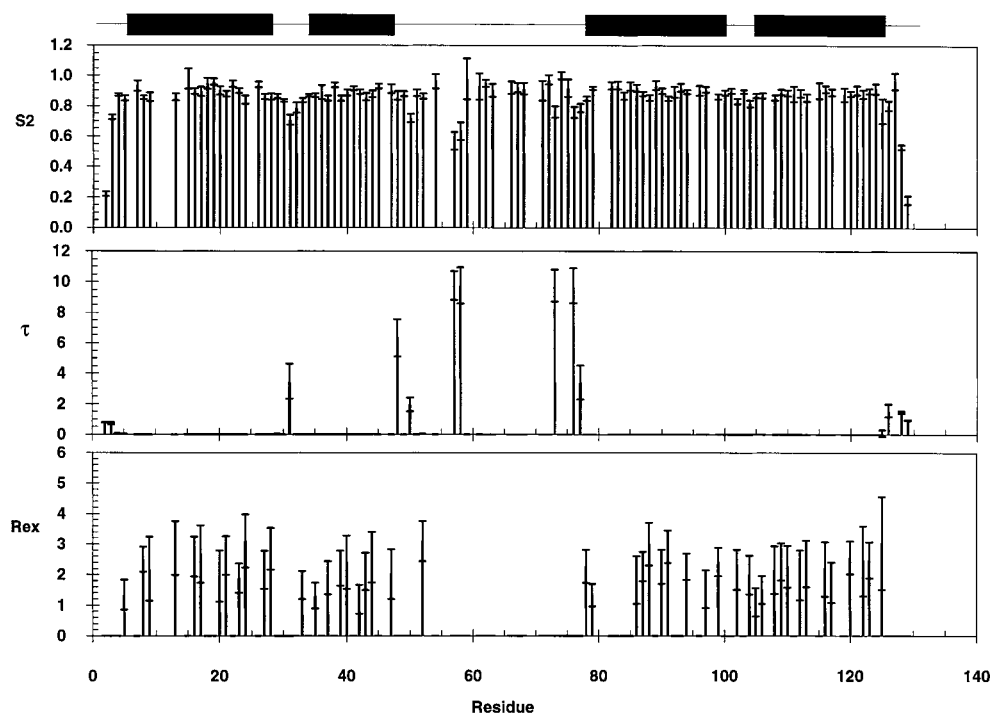


**Figure 2.** Dynamic parameters for cytochrome *c'* from *Rhodobacter capsulatus* assuming an isotropic rotational diffusion tensor: (Top) Order parameter,  $S^2$ , plotted against residue number and associated uncertainty (error bar). In the case of the extended Lipari–Szabo model,  $S^2 = S_i^2 S_s^2$ . (Middle) Internal correlation times  $\tau_1$  (ns) and associated uncertainty. (Bottom) Phenomenological chemical exchange contribution  $R_{ex}$  ( $s^{-1}$ ) and associated uncertainty.

**Characterization of Anisotropic Diffusion Tensor.** The shape of the cytochrome *c'* both as a monomer and in the dimeric form found in the crystal lattice implies that the molecule probably undergoes anisotropic rotational diffusion. We have therefore analyzed the anisotropy of the rotational diffusion tensor and investigated the statistical significance of the available models. Residues were selected for inclusion in the calculation on the basis of their presence in the secondary

structure, as these residues are most likely to undergo only rapid libration, which we treat as similarly negligible.<sup>12</sup> The results of the least-squares fitting of the measured  $R_2/R_1$  ratios using the isotropic and anisotropic spectral density functions given in eq 6 are shown in Tables 1–3. Note that the tensors optimized using the three-dimensional structures of the ligand-free (Table 2) and *n*-butyl isocyanide-bound (Table 1) forms of the protein are identical within the limits of the estimated uncertainty (the

**Table 1.** Axially Symmetric and Asymmetric Diffusion Parameters from  $R_2/R_1$  Using NBB-Ligated Structure (65 Vectors)

| tensor <sup>a</sup> | $D_{\parallel}/D_{\perp}$ | $D_{xx}^b$ ( $\times 10^7$ s <sup>-1</sup> ) | $D_{yy}$ ( $\times 10^7$ s <sup>-1</sup> ) | $D_{zz}$ ( $\times 10^7$ s <sup>-1</sup> ) | $\alpha^c$ (deg) | $\beta/\phi$ (deg) | $\gamma/\theta$ (deg) | $\chi_{\text{exp}}^2$ | $\chi_{0.05}^2$ <sup>d</sup> |
|---------------------|---------------------------|--|--|--|------------------|--------------------|-----------------------|-----------------------|------------------------------|
| ax. $m_2$           | 1.39 $\pm$ 0.03           | 1.510 $\pm$ 0.009                            | 1.510 $\pm$ 0.009                          | 2.11 $\pm$ 0.05                            | —                | -76.7 $\pm$ 2.0    | -37.5 $\pm$ 2.4       | 30.3                  | 80.5                         |
| ax. $m_1$           | 0.671 $\pm$ 0.03          | 1.26 $\pm$ 0.04                              | 1.88 $\pm$ 0.04                            | 1.88 $\pm$ 0.04                            | —                | 48.8 $\pm$ 4.4     | 48.4 $\pm$ 3.9        | 48.5                  | 80.4                         |
| asymm               | —                         | 1.37 $\pm$ 0.05                              | 1.68 $\pm$ 0.06                            | 2.13 $\pm$ 0.06                            | -35.8 $\pm$ 9.9  | -78.6 $\pm$ 2.2    | -33.1 $\pm$ 2.6       | 23.3                  | 77.9                         |

<sup>a</sup> All calculations were performed using the program TENSOR 1.0. Parameter uncertainties are taken from mean and standard deviations of MC simulations. Isotropic model gives  $D_{\text{iso}} = (1.59 \pm 0.01) \times 10^7$  s<sup>-1</sup> with  $\chi_{\text{exp}}^2 = 122.7$  compared to  $\chi_{0.05}^2 = 81.5$ ,<sup>d</sup> so this model is rejected. <sup>b</sup> The fitted parameters  $D_{\perp}$  and  $D_{\parallel}$  are shown here as  $D_{xx}$ ,  $D_{yy}$ , and  $D_{zz}$  for direct comparison with the asymmetric diffusion tensor. For the prolate approximation ( $m_2$ ),  $D_{\parallel} = D_{zz}$ ,  $D_{\perp} = D_{xx} = D_{yy}$ ; for the oblate approximation ( $m_1$ ),  $D_{\parallel} = D_{xx}$ ,  $D_{\perp} = D_{zz} = D_{yy}$ . <sup>c</sup> Angles ( $\alpha, \beta, \gamma$ ) describe the orientations of the structure frame in the frame of the diffusion tensor.  $D_{xx} < D_{yy} < D_{zz}$ . For axial symmetry, the polar angles  $\theta$  and  $\phi$  are given. <sup>d</sup>  $\chi_{0.05}^2$  refers to the ( $\alpha = 0.05$ ) confidence limit for the fit derived from 1000 MC simulations.

**Table 2.** Axially Symmetric and Asymmetric Diffusion Parameters from  $R_2/R_1$  Using Nonligated Cytochrome  $c'$  Coordinates

| tensor    | $D_{\parallel}/D_{\perp}$ | $D_{xx}$ ( $\times 10^7$ s <sup>-1</sup> ) | $D_{yy}$ ( $\times 10^7$ s <sup>-1</sup> ) | $D_{zz}$ ( $\times 10^7$ s <sup>-1</sup> ) | $\alpha$ (deg) | $\beta/\phi$ (deg) | $\gamma/\theta$ (deg) | $\chi_{\text{exp}}^2$ | $\chi_{0.05}^2$ |
|-----------|---------------------------|--|--|--|----------------|--------------------|-----------------------|-----------------------|-----------------|
| ax. $m_2$ | 1.393 $\pm$ 0.03          | 1.516 $\pm$ 0.009                          | 1.516 $\pm$ 0.009                          | 2.11 $\pm$ 0.07                            | —              | -85.7 $\pm$ 1.5    | -89.5 $\pm$ 2.8       | 38.9                  | 81.7            |
| ax. $m_1$ | 0.658 $\pm$ 0.03          | 1.25 $\pm$ 0.04                            | 1.90 $\pm$ 0.04                            | 1.90 $\pm$ 0.04                            | —              | 88.6 $\pm$ 4.8     | -4.25 $\pm$ 2.4       | 45.9                  | 81.9            |
| asymm     | —                         | 1.340 $\pm$ 0.04                           | 1.72 $\pm$ 0.05                            | 2.13 $\pm$ 0.07                            | 3.21 $\pm$ 8.6 | 87.0 $\pm$ 2.8     | 85.9 $\pm$ 2.0        | 27.1                  | 79.8            |

**Table 3.**  $F$  Statistic Calculated from Helical and Rigid Vector Data Sets Using Six-Parameter Fitting of Data Simulated from a Four-Parameter Model

| $\alpha$ | $F,^a$ ligated structure | $F$ , oxidized structure |
|----------|--------------------------|--------------------------|
|          |                          | Simulated                |
| 0.1      | 2.32                     | 1.83                     |
| 0.2      | 1.66                     | 1.41                     |
|          |                          | Experimental             |
|          | 8.73                     | 12.68                    |
| $p$      | $4.79 \times 10^{-4}$    | $2.63 \times 10^{-5}$    |

<sup>a</sup>  $F$ -test values between both the prolate four-parameter minima and the six-parameter model are shown.

orientation is, of course, different as the molecular frames are different in the two coordinate files).

**(A) Axially Symmetric Rotational Diffusion Tensor.** The dependence of the  $R_2/R_1$  ratio on the orientation of the NH vectors with respect to the unique axis of the prolate axially symmetric anisotropic diffusion tensor are shown in Figure 3a. As has recently been observed, two solutions exist when the tensor is truly anisotropic, representing prolate and oblate approximations of the system.<sup>45</sup> In the case for the cytochrome  $c'$ , we find that the prolate approximation reproduces the measured relaxation rate ratio much better than the oblate approximation ( $\chi_{\text{pro}}^2 = 30.3$  compared to  $\chi_{\text{obl}}^2 = 48.5$ ). As noted previously, the orientation of the unique axes of the oblate and prolate tensors is geometrically orthogonal.

Uncertainties in the eigenvalues and eigenvectors of the diffusion tensor have been determined using extensive Monte Carlo simulations. The errors cited in Tables 1–3 are taken from the standard deviations of these simulations. Given the extended nature of both monomeric and dimeric forms of the molecule, we were surprised to find that both axially symmetric minima were statistically acceptable as judged by the Monte Carlo derived 95% confidence levels ( $\chi_{0.05}^2 = 79.9$ ). The presence of these two significant minima implies that the axial symmetry is insufficient to describe the rotational diffusion and that the tensor is significantly rhombic. To test this hypothesis, we have modeled the rotational diffusion using the fully anisotropic form of the tensor.

**(B) Asymmetric Rotational Diffusion Tensor.** The anisotropic tensorial description  $\{D_{xx} = 1.37 \pm 0.05, D_{yy} = 1.68 \pm 0.06, D_{zz} = 2.13 \pm 0.07\} \times 10^7$  s<sup>-1</sup> is again statistically significant ( $\chi_{\text{exp}}^2 = 23.3, \chi_{0.05}^2 = 77.9$ ). The orientation of the

principal axes of the tensor, and their statistical distribution derived from the noise-simulated Monte Carlo data sets, are shown with respect to the molecule in Figure 4. The unique axis found for the prolate axial minimum is approximately reproduced by the component  $D_{zz}$ . The trace of the tensor is in close agreement with that used for the model-free analysis assuming isotropic diffusion.

We have tested the improvement relative to the lowest, prolate, minimum. The experimental  $F$  value is higher than the threshold for statistical significance of the improved fit ( $F_{0.10} = 2.52, F_{\text{exp}} = 8.73$ ). This is equivalent to a probability  $p = 4.79 \times 10^{-4}$  that the improvement is due to random statistics.

**Oligomerization State.** The accurate determination of the rotational diffusion parameters of the cytochrome  $c'$  suggests that its association state in solution can also be analyzed using the relaxation data. We have compared the orientation of the principal axes of the diffusion tensor with the principal components of the inertia tensor of the monomeric and dimeric forms of the molecule in the crystal lattice: in the case of a symmetric homodimer at least one of the axes of the diffusion tensor should be aligned with the symmetry axis of the crystal form. As shown in Figure 4, the axes are poorly aligned compared to the experimentally determined axis orientations, while there is very good agreement between the measured tensor and the inertia tensor of the monomeric form of the molecule. From this analysis it is possible to exclude that the molecule exists in solution as a homodimer with the relative orientation found in the crystal form (in this case, symmetry would be respected), and we propose that the molecule is very probably a monomer under the conditions of the NMR study. As far as we are aware, this is the first time such unambiguous information has been derived solely from NMR relaxation data.

This observation is of particular interest, as it can be correlated with the physicochemical characteristics of the RCCP M1131 strain: a recent study of the very similar RCCP M110 strain has shown that the association energy of this form is much lower than those for other cytochromes  $c'$ .<sup>30</sup> The M1131 strain also differs in the dimerization interface by the replacement of a hydrophobic residue Val38 with Ala, destabilizing the interaction with Ile46 in the other subunit, making dimerization energetically less attractive. Ligand-controlled dimer dissociation has been observed in the case of CVCP, where CO binding appears to be accompanied by cooperative monomer formation.<sup>31</sup> While the crystal structures of the ligand-free and  $n$ -butyl isocyanide-bound RCCP are both dimeric, our results show that the monomeric form is favored by the CO-bound state in solution,

(45) Blackledge, M. J.; Cordier, F.; Dosset, P.; Marion, D. *J. Am. Chem. Soc.* **1998**, *120*, 4538.

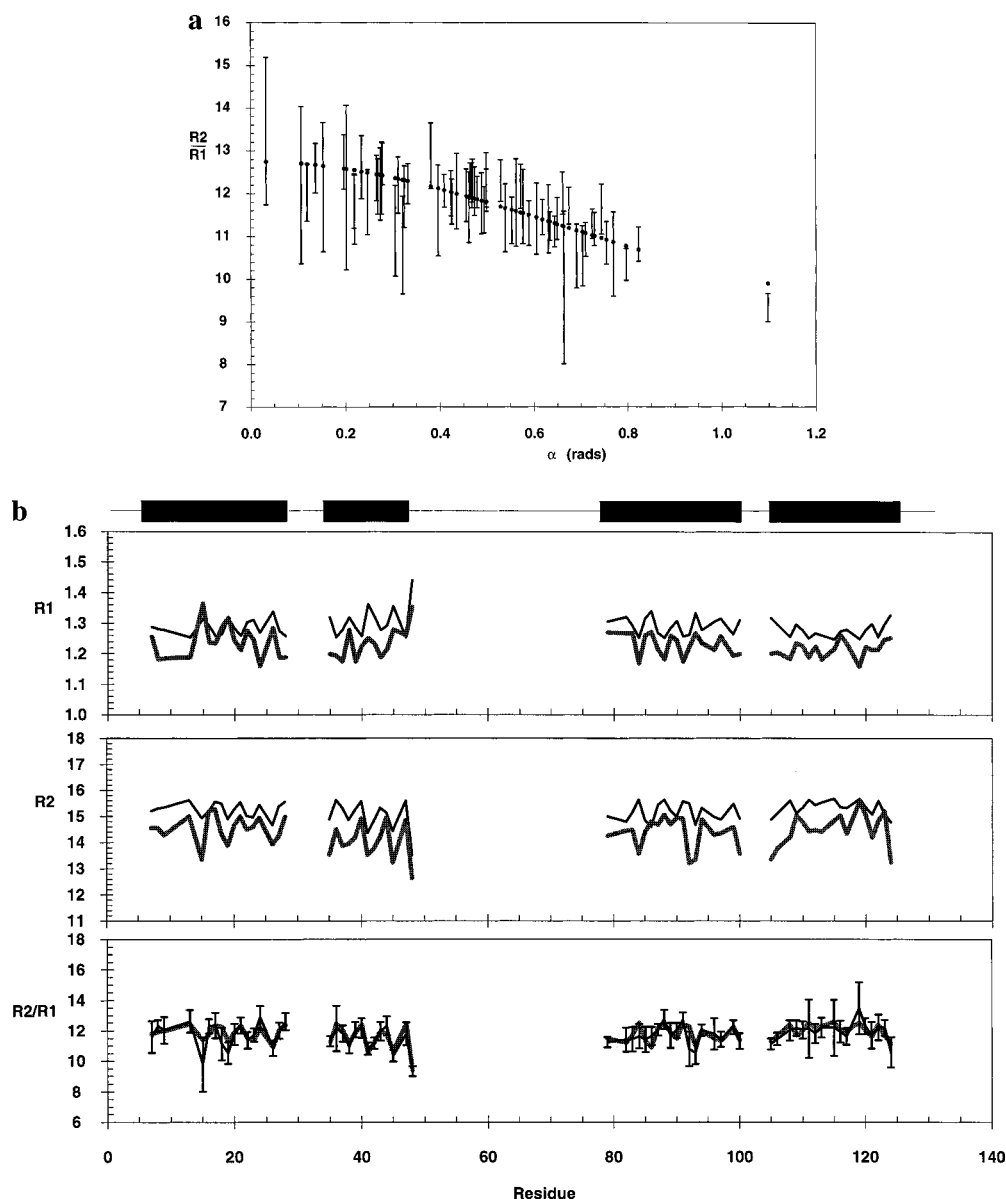


**Figure 3.** Experimental and model relaxation parameters. (a) Angular dependence of the ratio  $R_2/R_1$  for the NH vectors with respect to the unique axis of the axially symmetric diffusion tensor for the prolate minimum  $m_1$ . Points represent the best-fit model, while the error bars are centered on the experimental data. (b) (Bottom) Experimental and calculated  $R_2/R_1$  ratios for the NH vectors in helices with respect to primary sequence; experimental points are shown as the thick gray line, and the best-fit model calculated using the fully anisotropic diffusion tensor is shown as the thin line centered on error bars. The rest of the residues have been removed from the sequence for the sake of clarity. (Middle) Experimental and calculated  $R_2$  values for the NH vectors in helices with respect to primary sequence; experimental points are shown as the thick gray line, and the best-fit model calculated using the anisotropic diffusion tensor is shown as the thin line. Error bars have been removed for clarity; these are given in Figure 1. (Top) Experimental and calculated  $R_1$  values; experimental points are shown as the thick gray line, and the best-fit model calculated using the anisotropic diffusion tensor is shown as the thin line. The position of the helices with respect to the primary sequence is shown above the figure.

suggesting the existence of cooperative ligand binding for this form of the protein.

The absolute value of the diffusion tensor can also be compared with expected values based on the size and geometric form of the molecule. Hydrodynamic calculations performed using the coordinates of the monomeric form assuming a water shell of 3.0 Å gave values for the components of the diffusion tensor ( $D_{xx} = 1.42$ ,  $D_{yy} = 1.45$ ,  $D_{zz} = 2.12$ )  $\times 10^7$  s $^{-1}$  which are in approximate agreement with the relaxation data.

**Local Motion Assuming Anisotropic Tumbling.** The anisotropic diffusion tensor has been introduced into the Lipari–Szabo<sup>3</sup> spectral density function assuming anisotropic rotational diffusion (eq 8) to determine the local mobility in the protein (Figure 5). The dynamic behavior necessary to reproduce the

relaxation measurements is, in this case, strikingly simplified compared to the interpretation performed assuming isotropic diffusion. The cyclically dependent conformational exchange terms present in the helices are no longer present, and only one residue (Ala52) requires an  $R_{ex}$  term to adequately fit the relaxation data. It is also interesting to note that the  $S^2$  values no longer exhibit the cyclic fluctuations observed when the isotropic model is used. Both cyclic artifacts appear to be due to the varying orientation of the NH vectors with respect to the principal components of the rotational diffusion tensor, effects which are strikingly illustrated for the exchange contribution in Figures 2 and 5, and for the order parameter in helix III in Figure 6. Indeed, while the orientation of an N–H vector is often assumed to be coaxial with the direction of the  $\alpha$ -helix,

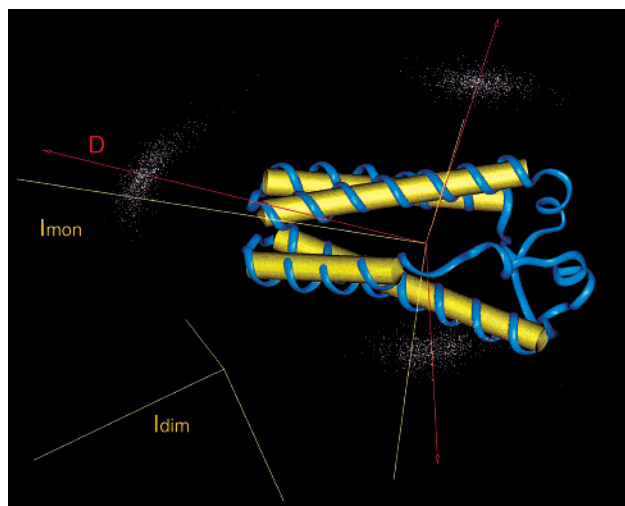


**Figure 4.** Relative orientations of the diffusion and inertia tensors. Orientation of the three principal axes of the asymmetric diffusion tensor. One thousand Monte Carlo simulations reproducing experimental uncertainty have been used to estimate the dispersion in the amplitude and orientation of the principal components of the diffusion tensor relative to the three-dimensional structure of the protein. The points represent the simulations, and the red lines represent the optimal tensor. The yellow lines represent the inertia tensor for the monomer (centered on the center of inertia of the molecule) and the crystallographic dimer (shifted from the center of inertia for clarity). The directions of the principal components of the tensor determined from hydrodynamic calculations are very similar to those derived from the inertia tensor.

this is, in fact, not the case. Vectors on different sides of an  $\alpha$ -helix have orientations which differ by  $2\lambda$ , where  $\lambda$  is the angle made by an NH vector and the axis of the helix, and consequently experience differential relaxation if the rotational diffusion tensor is significantly anisotropic. These observations are in contrast to previous propositions that the order parameter

of internal motion is largely independent of the model used to describe the rotational diffusion tensor.<sup>13</sup>

Using this analysis, the nonhelical regions present a total  $\chi^2$  value of  $26.9 \pm 1.0$ , compared to  $55.0 \pm 1.7$  obtained using the isotropic model, showing that internal mobility is also quantitatively improved in the regions which were not included in the modeling of the diffusion tensor. All helical residues assumed to be rigid for the optimization of anisotropic diffusion are adequately modeled with model 1. Thirteen residues are subject to internal motions on the slow time scale and three on a rapid time scale, while one residue (Ala73) marginally fails the statistical test for any of the available models ( $\chi^2 = 2.15$  for model 5).

**Comparison with Crystal Disorder.** The recent study of two polymorphs of RCCP suggested increased disorder, as measured by the average  $B$ -value, in the region Ala48–Leu54, which was contrasted with similar measurements from crystal structures of the homologous cytochromes  $c'$ , RMCP, CVCP, RRCP, and ADCP, where disorder was not observed, and was correlated with the identification of a channel in RCCP between the solvent and the heme pocket.<sup>25,30</sup> This channel is presumed to allow access of larger heme-binding ligands compared to other cytochromes  $c'$ , where the presence of bulky side chains blocks access to the heme. Our measurements do not confirm the presence of significantly greater amplitude subnanosecond motion in this region of the molecule, with the exception of Val51, although this does not preclude the presence of non-detected slower conformational disorder. More significant nanosecond time scale motion is found for the residues Gly58–Thr59, which form the base of the long loop region.

**Comparison of Measured and Calculated Relaxation Rates.** The high degree of precision available from the fit to the experimental  $R_2/R_1$  ratios also allowed us to investigate the predicted values of the relaxation rates  $R_2$  and  $R_1$  along the helices. This should allow us to identify local chemical exchange or internal motion, which may be artifactually interpreted as

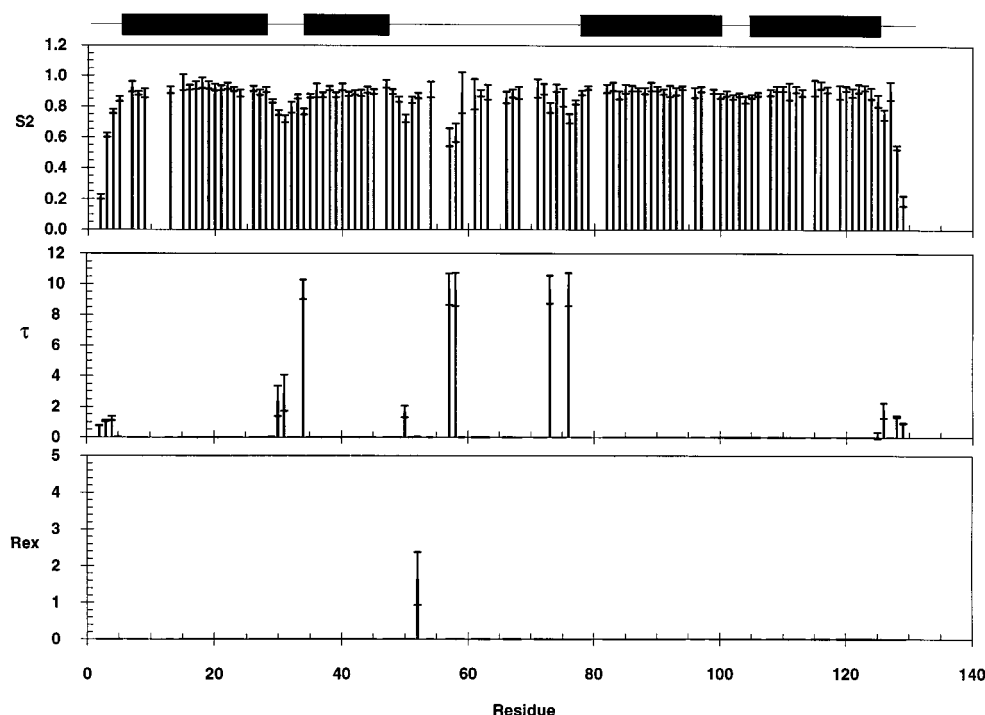


**Figure 5.** Dynamic parameters for cytochrome  $c'$  from *Rhodobacter capsulatus* assuming a fully anisotropic rotational diffusion tensor. (Top) Order parameter,  $S^2$ , plotted against residue number and associated uncertainty. (Middle) Internal correlation times  $\tau_1$  (ns) and associated uncertainty. (Bottom) Phenomenological chemical exchange contribution  $R_{ex}$  ( $s^{-1}$ ) and associated uncertainty.

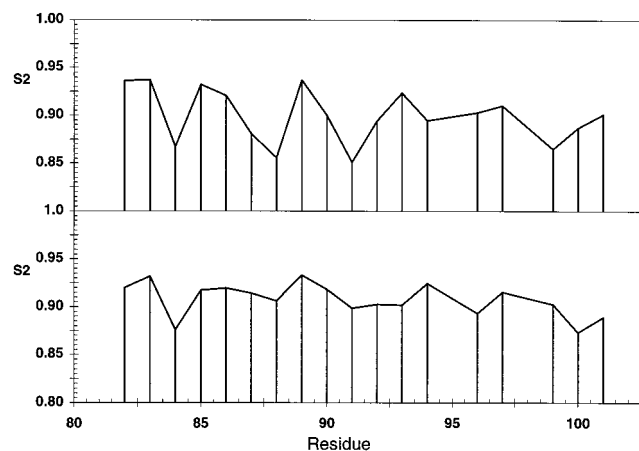


**Figure 6.**  $S^2$  profile for helix III derived from Lipari–Szabo analysis using isotropic (top) and anisotropic (bottom) rotational diffusion tensors.

anisotropic rotational diffusion in the  $R_2/R_1$  term, and which may remain undetected if only the ratio is investigated. This analysis also tests the validity of assuming a pervasive  $S^2$  value representing the internal mobility of all helical regions, as the ratio of the  $R_1$  and  $R_2$  calculated from the optimal diffusion tensor assuming an  $S^2$  of 1.0 ( $R_{\text{calc}}$ ) and the experimental values ( $R_{\text{meas}}$ ) should in this case be constant. The profile of the individual relaxation rates in helices II–IV are surprisingly accurately reproduced (Figure 3b), indicating that the differential relaxation effects are, indeed, due to anisotropic diffusion ( $R_1$  and  $R_2$  are both affected). The average ratio  $R_{\text{meas}}/R_{\text{calc}}$ , which is equivalent to an average order parameter in the librational limit, is  $0.880 \pm 0.003$ . Despite the very close agreement between the model and experimental values, helix I exhibits slightly different relaxation behavior from that predicted by the optimal tensor. While the periodicity predicted by the model is reproduced, the experimental relaxation rates are systematically higher, compared to the calculated values, than for the other three helices. Using the model-free approach, this effect is discernible as a higher average  $S^2$  term for helix I compared to those for the other three helices (Figure 5).

We have also optimized the tensor using  $R_2$  and  $R_1$  separately and a common  $S^2$  value which was simultaneously optimized as an additional parameter in the fit (data not shown). Not surprisingly, this gives a physically reasonable value of  $S^2 = 0.878 \pm 0.005$ . The tensor thus optimized is not different from that determined using the  $R_2/R_1$  ratio within the limits of the estimated error.

**Structure Refinement against  $R_2/R_1$ .** In view of the apparent high quality of the experimental relaxation data, we have attempted to optimize the structure of the CO-ligated cytochrome *c'* with respect to the local  $R_2/R_1$  ratio, starting from the known crystallographic coordinates of the butyl isocyanide-bound state.

The structure is minimized with respect to a target function that is dependent on both relaxation rates and a classical force field, leaving all atoms free to move, and assuming that the tensor determined using the crystallographic structure is approximately correct. The root-mean-square deviation of the backbone atoms with respect to the initial structure for the helical regions is  $0.80 \pm 0.10$ , and the average  $\chi^2$  target function of these structures is not significantly different from zero. The local root-mean-square deviation is shown in Figure 7a. As expected from the above, helix I reorientates slightly to fulfill the relaxation rates most significantly in the region covering the sixth ligand (residues Tyr13 and Leu17). This structural variation

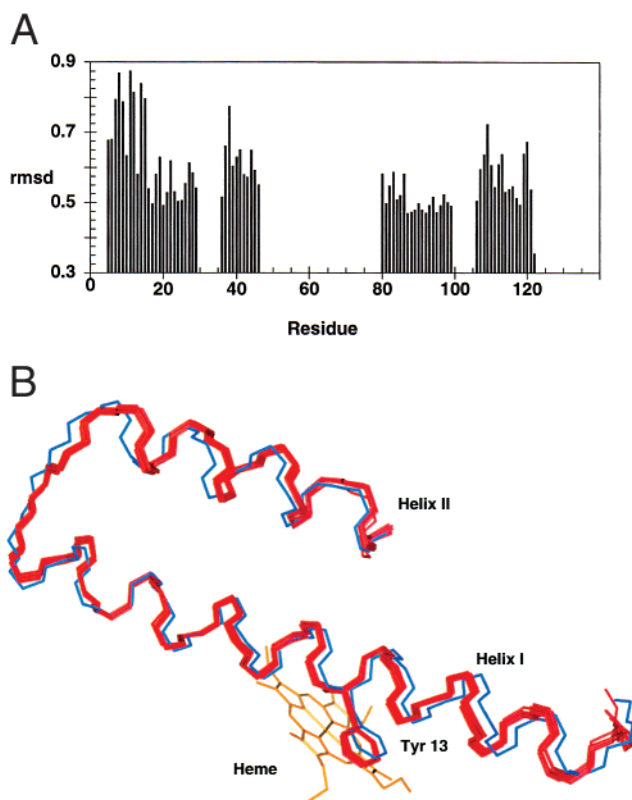


**Figure 7.** Structure refinement using relaxation rates. (a) Average backbone root-mean-square deviation (Å) between the crystal structure (1nbb) and the optimized structures as described in the text. Forty calculations are included in the statistics. (b) Graphical representation of the reorientation of helices I and II to accommodate the relaxation ratios. Ten structures from the optimization calculation are shown in red, and the crystal structure is shown in blue. Only one heme is shown for clarity.

may be explained by the difference between the experimentally studied form of the molecule, which is bound to CO as a sixth ligand, compared to the coordinates used for the tensor calculation which are from the crystal structure of the butyl isocyanide-bound cytochrome *c'*. Indeed, the helix can be seen to move closer to the heme in the structure refined against experimental data (Figure 7), an observation in agreement with the reduced volume of the sixth ligand in this form. The only other significant reorientation is observed for helix II, which moves slightly away from the helix cluster at its N-terminus. Although the distance involved in this reorientation is small (maximum backbone–backbone distance of 1.7 Å), it is possible that this is related to the different oligomerization states in the crystal and solution forms of the molecule, as this helix is strongly implicated in the dimerization site.<sup>30</sup>

These observations raise interesting questions concerning the local conformational differences between the differently ligated forms of the cytochrome *c'* of *Rhodobacter capsulatus*. We are, at present, in the process of determining the high-resolution three-dimensional structure of the CO-bound form of the protein in our laboratory using heteronuclear NMR spectroscopy.

## Conclusions

Heteronuclear relaxation measurements have been used to study the rotational diffusion and backbone dynamics of the carbon monoxide-bound *Rhodobacter capsulatus* cytochrome *c'*. Excellent agreement with experimental data is found if an anisotropic tensor is used to describe rotational diffusion. By direct comparison of the symmetry axes of the crystal state

structure with those of the rotational diffusion tensor in solution, we have been able to ascertain the oligomerization state of the protein in the bound state. While the crystal-state structures of the ligand-free and butyl isocyanide-bound forms of the molecule are dimeric, the  $^{15}\text{N}$  relaxation measurements have allowed us to prove that the CO-bound form is monomeric under the conditions used for the NMR investigation, providing evidence for either ligand-controlled cooperative dissociation or, alternatively, different crystalline/fully solvated oligomerization states.

The use of the anisotropic rotational diffusion tensor in the local relaxation analysis significantly improves the fitting of internal motion both qualitatively and quantitatively compared to the fit using the isotropic description of the tensor. In the case of the cytochrome *c'*, a predominantly prolate molecule, residues in helices aligned with the long axis of the tensor can thus be modeled using a simple librational motion, whereas they require significant cyclically varying chemical exchange components and order parameters if isotropic rotational diffusion is assumed.

The high precision of the relaxation data presented here is manifest in the precision with which the diffusion tensor can

be determined and has allowed the optimization of the three-dimensional coordinates of the butyl isocyanide-bound crystallographic structure to propose an initial model for the structure of the CO-bound form, which is under further investigation in our laboratory.

**Acknowledgment.** The authors acknowledge the indispensable programming skills of Patrice Dosset. Pierre Gans, H el ene D em en e, Jean-Pierre Simorre, and Bernhard Brutscher are acknowledged for helpful discussions. Prof. A. Arseniev is gratefully acknowledged for the use of the program DIFFC in the package DASHA. This project was supported by the Commissariat   l' nergie Atomique and the CNRS. This work is part of a continued collaboration with Molecular Simulations Incorporated. This is publication no. 900 of the Institut de Biologie Structurale.

**Supporting Information Available:** One table containing experimental  $^{15}\text{N}$  relaxation data for the 106 resolved  $^{15}\text{N}$ – $^1\text{H}$  peaks in the HSQC spectrum (PDF). This material is available free of charge via the Internet at <http://pubs.acs.org>.

JA993654K